
Learned D-AMP: A Principled CNN-based Compressive Image Recovery Algorithm

Christopher A. Metzler
Rice University
chris.metzler@rice.edu

Ali Mousavi
Rice University
ali.mousavi@rice.edu

Richard G. Baraniuk
Rice University
richb@rice.edu

Abstract

Compressive image recovery is a challenging problem that requires fast and accurate algorithms. Recently, neural networks have been applied to this problem with promising results. By exploiting massively parallel GPU processing architectures and oodles of training data, they are able to run orders of magnitude faster than existing methods. Unfortunately, these methods are difficult to train, often-times specific to a single measurement matrix, and largely unprincipled blackboxes.

It was recently demonstrated that iterative sparse-signal-recovery algorithms can be “unrolled” to form interpretable deep neural networks. Taking inspiration from this work, we develop novel neural network architectures that mimic the behavior of the denoising-based approximate message passing (D-AMP) and denoising-based vector approximate message passing (D-VAMP) algorithms. We call these new networks *Learned D-AMP* (LDAMP) and *Learned D-VAMP* (LDVAMP).

The LDAMP/LDVAMP networks are easy to train, can be applied to a variety of different measurement matrices, and come with a state-evolution heuristic that accurately predicts their performance. Most importantly, our networks outperform the state-of-the-art BM3D-AMP and NLR-CS algorithms in terms of both accuracy and runtime. At high resolutions, and when used with matrices which have fast matrix multiply implementations, LDAMP runs over $50\times$ faster than BM3D-AMP and hundreds of times faster than NLR-CS.

1 Introduction

Over the last few decades computational imaging systems have proliferated to a host of different imaging domains. From synthetic aperture radars applied to remote sensing to functional MRIs and CT scanners applied to medical imaging, computational imaging systems have become commonplace. The majority of these systems capture linear measurements which can be modeled by the equations $y = \mathbf{A}x + \epsilon$ where $x \in \mathbb{R}^n$ denotes the signal of interest, $\mathbf{A} \in \mathbb{R}^{m \times n}$ denotes the measurement matrix, $y \in \mathbb{R}^m$ denotes the measurements, and $\epsilon \in \mathbb{R}^m$ denotes the noise.¹

Computational imaging systems seek to take measurements y of this form, along with knowledge of the measurement matrix \mathbf{A} , and recover x . When $m < n$ this problem is underdetermined and prior knowledge about x must be used to reconstruct the signal. This problem is broadly referred to as compressive sampling (CS) [1; 2].

Recovering compressively sampled images presents two central challenges. First, the dimensions of typical images are on the order of hundreds of thousands to millions. Thus any algorithm that we hope to run in anywhere close to real time must be extremely efficient. Second, images have

¹Analogous equations can be written when dealing with complex-valued signals and measurements.

complicated structures which necessitate sophisticated priors. Simple models like sparsity produce poor reconstructions [3].

Recently neural networks (NN) have made strides towards solving both of these problems [4–10]. First, through the effective use of massively parallel GPU architectures they are able to run orders of magnitude faster than existing compressive image recovery methods. Second, by using vast amounts of training data they are able to implicitly learn accurate models for natural images.

Unfortunately, NNs come with drawbacks. They are difficult to train, often-times specific to a single measurement matrix, and largely unprincipled blackboxes. This work rectifies these problems by creating networks that mimic the behavior of Denoising-based AMP (D-AMP) [3] and Denoising-based VAMP (D-VAMP) [11]; algorithms with exceptional performance and well known characteristics.

The inspiration for this work comes from the LISTA [12; 13] and LAMP/LVAMP [14] neural networks. In these works, the authors unroll the iterative ISTA [15] and AMP/VAMP [16; 17] algorithms, respectively, and then treat parameters of the algorithm as weights to be learned. In this way, an algorithm consisting of L iterations become a neural network with L layers. We do the same to D-AMP and D-VAMP to form Learned D-AMP (LDAMP) and Learned D-VAMP (LDVAMP). However, whereas the LISTA and LAMP/LVAMP networks efficiently recover compressively sampled sparse signals, LDAMP and LDVAMP recover compressively sampled images.

Because they are based off of the well understood D-AMP and D-VAMP algorithms, LDAMP/LDVAMP are easy to train, can be applied to a variety of different measurement matrices, and come with a state-evolution heuristic that accurately predicts their performance. Most importantly, LDAMP/LDVAMP outperform the state-of-the-art BM3D-AMP and NLR-CS algorithms in terms of both accuracy and runtime. At high resolutions, when used with matrices which have fast matrix multiply implementations, LDAMP runs over $50\times$ faster than BM3D-AMP and hundreds of times faster than NLR-CS.

2 Related Work

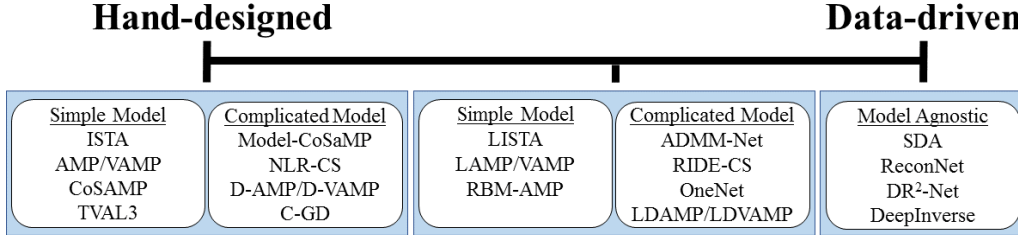


Figure 1: The spectrum of signal recovery algorithms spans from hand-designed algorithms to completely data-driven approaches.

The CS problem is to recover a signal from a set of undersampled linear measurements. More explicitly, we are interested in recovering $x \in \mathbb{R}^n$ from $y = \mathbf{A}x + \epsilon$ where $\mathbf{A} \in \mathbb{R}^{m \times n}$ and $m \ll n$. This problem is under-determined and thus we are able to recover x only if it has some type of structure that allows its dimensionality to be reduced without losing information [1; 2].

There are myriad ways to use priors on x 's structure to recover the signal. In the following we briefly describe some of these methods. Note that the ways in which these algorithms use priors on x 's structure span a spectrum; from simple hand-designed models to completely data-driven methods (Figure 1).

2.1 Hand-designed

The vast majority of CS recovery algorithm can be considered “hand-designed” in the sense that they use some sort of expert knowledge, i.e., prior, about the structure of x . The most common signal prior is that x is sparse in some basis. Following this model, one often recovers x by setting

up an optimization problem that applies a convex ℓ_1 penalty on the coefficients of x . To solve this convex problem, researchers often use linear programming [18] or iterative algorithms, e.g. ISTA [15], AMP [16], and VAMP [17]. Numerous greedy methods also try to solve the sparse recovery problem directly, without using an ℓ_1 relaxation, e.g., CoSaMP [19].

While useful as a proof of concept, algorithms that use only a sparsity prior struggle to recover compressively sampled images. The reason for this failure is that images are not exactly sparse in any basis. For this reason, researchers designed more elaborate priors such as minimal total variation, e.g., TVAL3 [20], markov-tree models on the wavelet coefficients, e.g., Model-CoSaMP [21], and nonlocal self-similarity, e.g., NLR-CS [22]. More recently, highly developed denoising and compression algorithms have been used to impose priors on the reconstructions, e.g., D-AMP [3] and C-GD [23].

The appeal of hand-designed methods is that they are based on interpretable priors and often have well understood behavior. Moreover, when they are set up as convex optimization problems they often have theoretical convergence guarantees. Unfortunately, among the algorithms that use accurate priors on the signal, even the fastest [3] is too slow for many real-time applications. More importantly, these algorithms do not take advantage of any training data. As we will see, this leaves a large room for improvement.

2.2 Data-driven

On the other end of the spectrum, researchers have recently developed compressive recovery algorithms that use no hand-designed models whatsoever. That is, the algorithms themselves are completely agnostic to any prior we might have about the signal. Instead, researchers provided neural networks vast amounts of training data, and the algorithms learn how to best use the structure within the data [4; 5; 7; 6].

The first paper to study this approach was [4] where authors used stacked denoising autoencoders (SDA) to recover signals from their undersampled measurements. Other papers in this line of work use either pure convolutional layers [6] or a combination of convolutional and fully-connected layers [7; 5] to build deep learning frameworks capable of solving the CS recovery problem. As demonstrated in [4], signal recovery based on deep learning frameworks can compete with state-of-the-art methods in terms of accuracy while running thousands of times faster. Unfortunately, these methods are held back by the fact that there exists almost no theory governing their performance and that, so far, they must be trained for specific measurement matrices and noise levels.

2.3 Mixing Hand-designed and Data-driven Methods

The third class of recovery algorithms blends data-driven models with hand-designed algorithms. That is, they first use expert knowledge to set up a recovery algorithm and then use training data to learn priors within this algorithm. In this way, such methods benefit from training data, while still potentially maintaining the interpretability and guarantees that made hand-designed methods so appealing.

Algorithms of this class can be divided into two subcategories. The first subcategory treat NNs as blackboxes that perform some function within the algorithm; such as proximal mapping. The second subcategory explicitly unroll iterative algorithm and turn them into a neural net. Following this unrolling, the network can be tuned with training data. Our LDAMP/LDVAMP algorithms uses ideas from both these camps.

2.3.1 Blackbox Neural Nets

The simplest way to use a NN in a principled way to solve the CS problem is to treat it as a blackbox that performs some function; such as computing a posterior probability.

The first examples of this approach showed up in a series of works, [24–26], which integrated Restricted Boltzmann Machines (RBM) into the AMP algorithm. The resulting algorithms, RBM-AMP and its generalizations, use RBMs to learn and apply non-i.i.d. priors to solve the CS problem. When trained on the MNIST dataset, the algorithms were able to successfully model and use the correlations within images of handwritten digits.

The second example of this approach was [9], which we denote as RIDE-CS. In this work the authors used the RIDE [27] generative model to compute the probability of a given estimate of the image. This enabled them to use gradient ascent on the signal’s posterior distribution to reconstruct images from compressive measurements.

The third method, which we denote OneNet [10], use ADMM [28] to solve several imaging inverse problems including inpainting, denoising, and CS. This method uses a NN as a proximal mapping, and can be interpreted as a NN-based version of Plug and Play ADMM [29]. Using a NN in this way allows the authors to derive useful convergence guarantees.

2.3.2 Unrolled Algorithms

The second principled technique to use a NN to solve the CS problem is to simply take a well-understood algorithm and unroll/unfold it. This method is best illustrated by the LISTA [12; 13] and LAMP [14] neural networks. In these works, the authors simply unroll the iterative ISTA [15] and AMP [16] algorithms, respectively, and then treat parameters of the algorithm as weights to be learned. One can parameterize the matrices \mathbf{A} and \mathbf{A}^H [12], the nonlinearities $\eta_\theta(\cdot)$ [13], or both [14].

Approximate Message Passing (AMP)

$$\begin{aligned} z^t &= y - \mathbf{A}\hat{x}^t + \frac{\|\hat{x}^t\|_0}{m} z^{t-1}, \\ \hat{x}^{t+1} &= \eta_{\theta^t}(\hat{x}^t + \mathbf{A}^H z^t; \frac{\|z^t\|_2}{\sqrt{m}}). \end{aligned}$$

Learned AMP (LAMP)

$$\begin{aligned} z^0 &= y - \mathbf{A}\hat{x}^0 \\ \hat{x}^1 &= \eta_{\theta^1}(\hat{x}^0 + \mathbf{A}^H z^0; \frac{\|z^0\|_2}{\sqrt{m}}), \\ z^1 &= y - \mathbf{A}\hat{x}^1 + \frac{\|\hat{x}^1\|_0}{m} z^0, \\ \hat{x}^2 &= \eta_{\theta^2}(\hat{x}^1 + \mathbf{A}^H z^1; \frac{\|z^1\|_2}{\sqrt{m}}), \\ &\vdots \\ \hat{x}^L &= \eta_{\theta^L}(\hat{x}^{L-1} + \mathbf{A}^H z^{L-1}; \frac{\|z^{L-1}\|_2}{\sqrt{m}}). \end{aligned}$$

To be concrete, consider AMP and LAMP. In the AMP algorithm $\eta(\cdot)_{\theta^t}$ is some simple nonlinearity, such as soft-thresholding, parameterized by θ^t . The terms x^t and z^t are the estimates of the signal x and the residual z at iteration t . In the LAMP network, the authors simply unroll the iterations of AMP. The equations to the right now define a neural network. Training data can be fed through it and stochastic gradient descent can be used to update and optimize its parameters $\theta^0, \theta^1, \dots$.

Unrolling was recently applied to the ADMM algorithm to solve the CS-MRI problem [8]. The resulting network, ADMM-Net, used training data to learn filters, penalties, simple nonlinearities, and multipliers. Moving beyond CS, the unrolling principle has been applied successfully to speech enhancement [30], non-negative matrix factorization applied to music transcription [31], and more. In all these applications unrolling and training can significantly improve both the quality and speed of reconstructions.

3 Learned D-AMP

In this section we first briefly review the denoising-based iterative thresholding (D-IT) and denoising-based AMP (D-AMP) [3] algorithms. We then describe the denoising convolutional neural network (DnCNN) image denoiser [32]. Finally, we describe how D-IT and D-AMP can be unrolled and combined with the DnCNN denoiser to form Learned D-IT (LDIT) and Learned D-AMP (LDAMP).

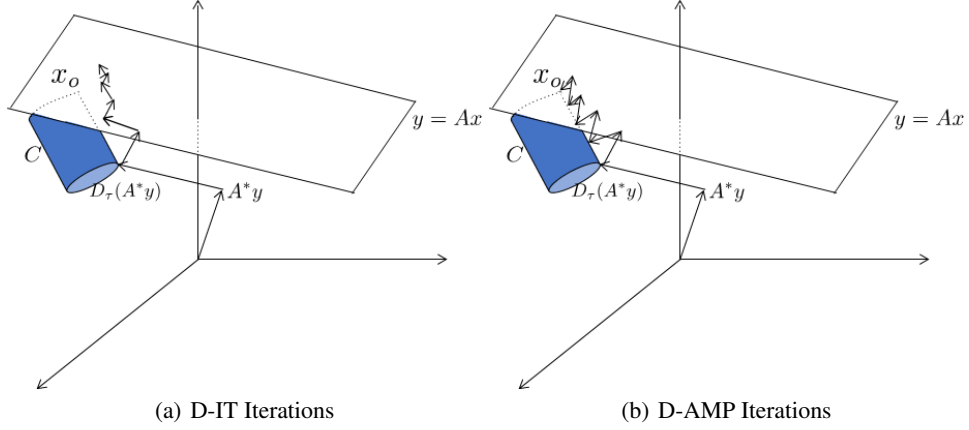


Figure 2: Idealized reconstruction behavior of D-IT (left) and D-AMP (right). Because D-IT allows bias to build up over iterations of the algorithm, its denoiser becomes ineffective at projecting onto the set C of all natural images. The Onsager correction term allows D-AMP to avoid this issue. Figure adapted from [3].

3.1 Denoising-based IT

Denoising-based Iterative Thresholding (D-IT)

$$\begin{aligned} z^t &= y - \mathbf{A}x^t, \\ x^{t+1} &= D_{\sigma^t}(x^t + \mathbf{A}^*z^t). \end{aligned} \quad (1)$$

To understand the D-IT and D-AMP algorithms, it helps to formulate the compressive imaging problem as follows. Let C denote the set of all natural images. A compressive image recovery algorithm should find the natural image x that best matches the observations y . Thus, the algorithms should solve

$$\operatorname{argmin}_x \|y - \mathbf{A}x\|_2^2 \text{ subject to } x \in C. \quad (2)$$

When no measurement noise is present, a compressive image recovery algorithm should return the (hopefully unique) point x_o that intersects the set C and the affine subspace $\{x|y = \mathbf{A}x\}$, illustrated in Figure 2.

The premise of D-IT and D-AMP is that high-performance image denoisers D_σ , like BM3D [33], are approximately projecting onto the set C of all natural images.² That is, suppose $x_o + \sigma z$ is a noisy observation of a natural image; $x_o \in C$ and $z \sim N(0, 1)$. An ideal denoiser D_σ would simply find the point in the set C closest to the observation $x_o + \sigma z$. That is

$$D_\sigma(x) = \operatorname{argmin}_x \|x_o + \sigma z - x\|_2^2 \text{ subject to } x \in C. \quad (3)$$

The aforementioned interpretations of the compressive image recovery and image denoising problems, (2) and (3) respectively, lead naturally to the denoising-based iterative thresholding (D-IT) algorithm, presented in (1) and illustrated in Figure 2. The D-IT algorithm proceeds as follows: Starting from $x^0 = 0$, take a gradient step towards the $\{x|y = \mathbf{A}x\}$ affine subspace. Next apply the denoiser D_σ to move into the set C of natural images. Starting from your previous estimate, repeat.

Let $\nu^t = x^t + \mathbf{A}^*z^t - x_o$; the difference between $x^t + \mathbf{A}^*z^t$ and the true signal x_o at each iteration. ν^t is known as the effective noise. At each iteration, D-IT denoises $x^t + \mathbf{A}^*z^t = x_o + \nu^t$; it denoises the true signal plus ν^t . Most denoisers implicitly model ν^t as additive white Gaussian noise (AWGN).

²We use the notation D_σ to indicate that the denoiser can be parameterized by the standard deviation of the noise.

Unfortunately, as D-IT iterates, the denoiser biases the intermediate solutions and ν^t no longer resembles AWGN. This behavior is best demonstrated with iterative soft-thresholding (IST) [34], the simplest version of D-IT. IST has a well documented behaviour of producing heavy-tailed, nongaussian effective noise [16; 3; 14]. D-AMP differs from D-IT in that it corrects for this bias at each iteration.

3.2 Denoising-based AMP

Denoising-based Approximate Message Passing (D-AMP)

$$\begin{aligned} z^t &= y - \mathbf{A}x^t + \frac{1}{m}z^{t-1}\text{div}D_{\hat{\sigma}^{t-1}}(x^{t-1} + \mathbf{A}^*z^{t-1}), \\ \hat{\sigma}^t &= \frac{\|z^t\|_2}{\sqrt{m}}, \\ x^{t+1} &= D_{\hat{\sigma}^t}(x^t + \mathbf{A}^*z^t). \end{aligned} \tag{4}$$

D-AMP, presented in (4), is no more than the D-IT algorithm plus an Onsager correction term; $z^{t-1}\frac{\text{div}D_{\hat{\sigma}^{t-1}}(x^{t-1} + \mathbf{A}^*z^{t-1})}{m}$.³ This Onsager correction term removes bias from the intermediate solutions so that the effective noise ν^t follows the AWGN model expected by typical image denoisers. For more information on the Onsager correction and where it comes from see [16]. Note that $\frac{\|z^t\|_2^2}{m}$ serves as useful and accurate estimate of the variance of ν^t [35].

Typically D-AMP refers to algorithms that use the following Monte-Carlo approximation for the divergence $\text{div}D(\cdot)$, first introduced in [36; 3].⁴

Given a denoiser $D_{\hat{\sigma}}(x)$, using an i.i.d. random vector $b \sim N(0, I)$, we can estimate the divergence with

$$\begin{aligned} \text{div}D_{\hat{\sigma}} &= \lim_{\epsilon \rightarrow 0} E_b \left\{ b^* \left(\frac{D_{\hat{\sigma}}(x + \epsilon b) - D_{\hat{\sigma}}(x)}{\epsilon} \right) \right\} \\ &\approx \mathbb{E} \left(\frac{1}{\epsilon} b^* (D_{\hat{\sigma}}(x + \epsilon b) - D_{\hat{\sigma}}(x)) \right), \text{ for very small } \epsilon. \end{aligned} \tag{5}$$

To compute this expected value we can use Monte Carlo sampling:

$$\text{div}\hat{D}_{\hat{\sigma}^t} = \frac{1}{M} \sum_{i=1}^M \widehat{\text{div}}^i,$$

where $\widehat{\text{div}}^i$ is the estimate of the divergence from the i^{th} Monte Carlo sample. In this work set $\epsilon = \frac{\|x\|_{\infty}}{1000}$ and $M = 1$. For more information on this approximation see [3].

3.3 Denoising Convolutional Neural Network

Neural networks have been used for denoising for some time, see for instance [37]. However, only recently have they begun to significantly outperform established methods like BM3D [33]. In this section we review the recently developed Denoising Convolutional Neural Network (DnCNN) image denoiser, which is simultaneously more accurate and far faster than competing techniques [32].

The DnCNN neural network is illustrated in Figure 3. It consists of 16 to 20 convolutional layers, organized as follows. The first convolutional layer uses 64 different $3 \times 3 \times c$ filters (where c denotes the number of color channels) and is followed by a rectified linear unit (ReLU) [38]. Its next 14 to 18 convolutional layers each use 64 different $3 \times 3 \times 64$ filters which are each followed by batch-normalization [39] and a ReLU. The final convolutional layer uses c separate $3 \times 3 \times 64$ filters

³ $\text{div}D(\cdot)$ denotes the divergence of the denoiser. This is simply the sum of its partial derivatives with respect to x .

⁴When the divergence can be computed analytically D-AMP is just AMP.

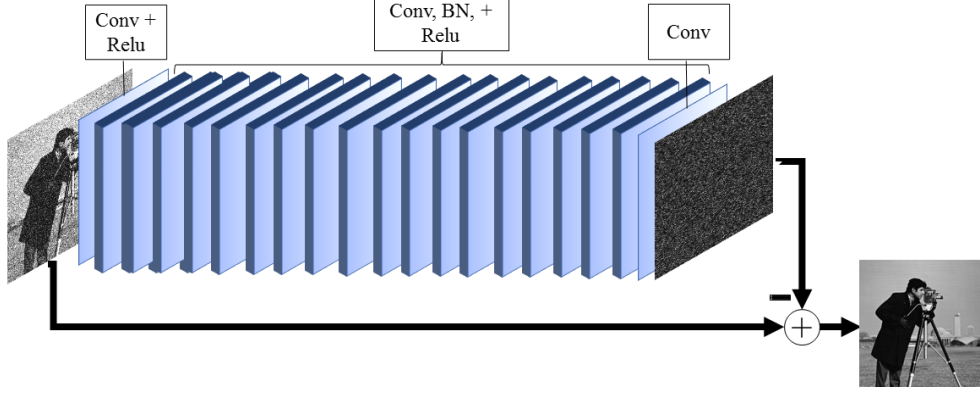


Figure 3: Network architecture of the DnCNN denoiser [32]. Notice it first estimates the residual, rather than the denoised image itself.

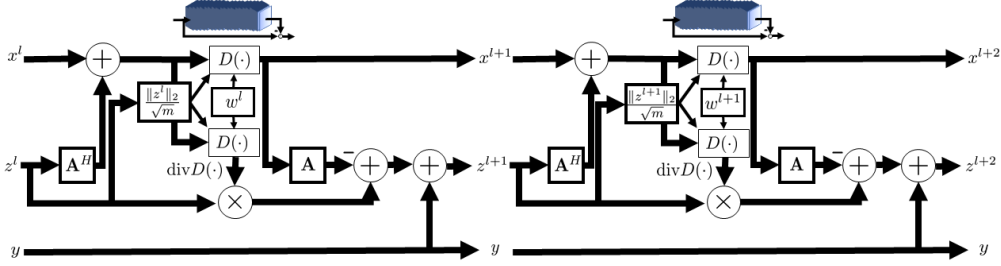


Figure 4: Two layers of the LDAMP neural network. When used with the DnCNN denoiser each denoiser block is a 20 convolutional-layer neural network. The forward and backward operators are represented as matrices \mathbf{A} and \mathbf{A}^H , however function handles work as well.

to reconstruct the signal. Throughout the rest of this paper, we will use the 20 layer version of the DnCNN network.

Rather than learning a mapping from a noisy image to a denoised image directly, the DnCNN authors found it beneficial to learn the residual vector. That is, in the context of the denoising problem (3), the network is given $x_o + \sigma z$ as an input and produces \hat{z} , not \hat{x}_o , as an output. This method, known as residual learning [40], sets up the network to remove the highly structured natural image, rather than the unstructured noise; an easier problem. As a result, residual learning improves both the training times and accuracy of the network.

3.4 Unrolling D-IT and D-AMP

The central contribution of this work is to take the unrolling ideas behind LISTA [12; 13] and LAMP [14] and apply them to D-IT and D-AMP. To reiterate, in [12; 13] and [14] the authors unroll the iterative ISTA [15] and AMP [16] algorithms, respectively, and then treat parameters of the algorithm as weights to be learned. In this way, an algorithm consisting of L iterations become a neural network with L layers. Here we do the same to D-IT and D-AMP to form LDIT and LDAMP. However, whereas the LISTA and LAMP networks efficiently recover compressively sampled sparse signals, LDIT and LDAMP recover compressively sampled images.

The LDAMP network, presented in (6) and illustrated in Figure 3.4 consists of 10 AMP layers. Each AMP layers contains two denoisers with tied weights. One denoiser is used to updated x^l and the other is used to estimate the divergence using the Monte-Carlo approximation described in Section 3.2. The LDIT network is nearly identical but does not need to compute an Onsager correction term and so only applies one denoiser per layer.

One of the few challenges to unrolling D-IT and D-AMP is that to enable training we must use a denoiser that easily propagates gradients; a blackbox denoiser like BM3D will not work. This restricts us to denoisers such as DnCNN, which fortunately offer the best performance.

Learned Denoising-based Approximate Message Passing (LDAMP)

$$\begin{aligned} z^l &= y - \mathbf{A}x^l + \frac{1}{m}z^{l-1}\text{div}D_{w^l(\hat{\sigma}^l)}^{l-1}(x^{l-1} + \mathbf{A}^*z^{l-1}), \\ \hat{\sigma}^l &= \frac{\|z^l\|_2}{\sqrt{m}}, \\ x^{l+1} &= D_{w^l(\hat{\sigma}^l)}^l(x^l + \mathbf{A}^*z^l). \end{aligned} \tag{6}$$

Within (6) we use a slightly cumbersome notation $D_{w^l(\hat{\sigma}^l)}^l$ to indicate that layer l uses denoiser D^l , that this denoiser depends on its weights w^l , and that these weights may be a function of the estimated standard deviation of the noise $\hat{\sigma}^l$. In practice one need not use a different denoiser at different layers, and in fact we found it easiest to train and use a single denoiser, whose weights were set by $\hat{\sigma}^l$, for all the layers.

During training the only free parameters we maintained in the network were the denoiser weights w^1, \dots, w^L . This is distinct from the LISTA and LAMP networks, where the authors decouple the \mathbf{A} and \mathbf{A}^H matrices used in the network from the true measurement matrix, which may not be exactly known, and learn them on a layer-by-layer basis [12; 14]. Because our focus is on high-dimensional imaging problems, where the measurement matrices can have many millions of elements, we did not pursue this direction and kept our forward and backward operators, \mathbf{A} and \mathbf{A}^H known and fixed. In [13] the authors also fixed \mathbf{A} and \mathbf{A}^H and just optimized the nonlinearities used in the LISTA network.

A similar unrolling process can be applied to Denoising-based Vector AMP (DVAMP) [11] to form Learned DVAMP (LDVAMP). DVAMP is a variant of D-AMP that functions with a broader class of measurement matrices.

4 Theoretical Analysis

This work makes three theoretical contributions. First, we demonstrate the state evolution heuristic, a series of equations that predict the performance of D-AMP and D-VAMP, holds for LDAMP and LDVAMP as well. Second, we use the state evolution to prove that layer-by-layer training of LDAMP/LDVAMP is mean-squared error (MSE) optimal. Finally, we prove that in the context of dense i.i.d. Gaussian measurement matrices, the DnCNN variant of LDAMP has a provably low computational complexity.

4.1 State Evolution

The AMP/D-AMP state evolution is a series of equations that predicts the performance of the algorithm over each of its iterations [16; 41; 3]. In the context of LAMP/LVAMP and LDAMP/LDVAMP the equations predict the performance of the network over each of its layers [14]. In this section we review the state evolution and present our main theoretical finding; the state evolution holds for LDAMP and LDVAMP.

Note that the state evolution we provide here is the “deterministic” state-evolution proposed in [3] to predict the performance of D-AMP. This state-evolution is distinct from the widely studied “probabilistic” state-evolution proposed in [16], proven, for some contexts, in [41], and verified for LAMP and LVAMP in [14]. The “deterministic” state evolution fixes the signal x_o and takes the expectation over the distribution of the noise. By contrast, the “probabilistic” state evolution takes the expectation over the distribution of both the signal and the noise vector.

Starting from $\theta^0 = \frac{\|x_o\|_2^2}{n}$ the state evolution generates a sequence of numbers through the following iterations:

$$\theta^{l+1}(x_o, \delta, \sigma_\epsilon^2) = \frac{1}{n}\mathbb{E}\|D_{w^l(\sigma)}^l(x_o + \sigma^l\epsilon) - x_o\|_2^2, \tag{7}$$

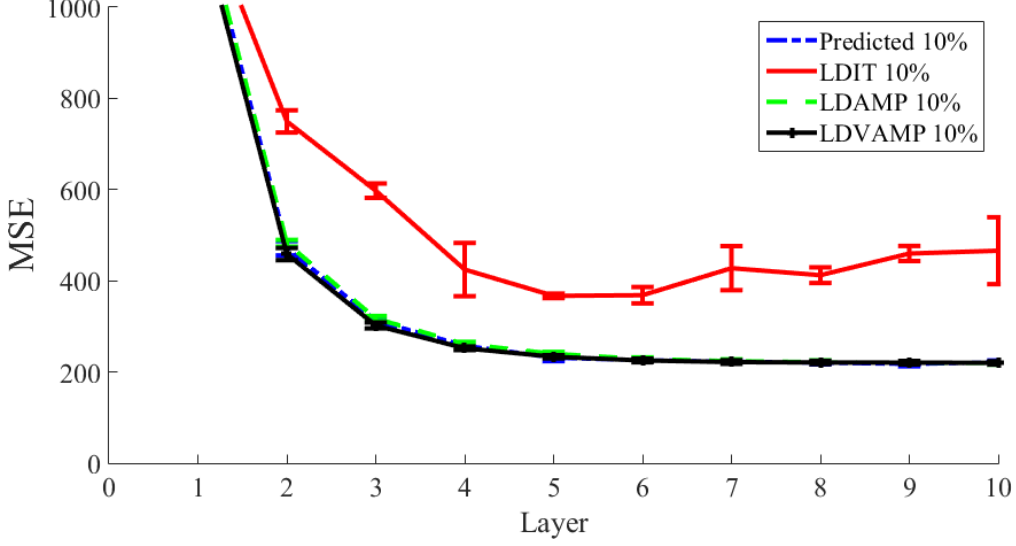


Figure 5: The MSE of intermediate reconstructions of a 10% sampled House image across different layers for the DnCNN variants of LDAMP, LDVAMP, and LDIT alongside their predicted state evolution. Notice that LDAMP and LDVAMP are well predicted by the state evolution whereas LDIT is not.

where $(\sigma^l)^2 = \frac{1}{\delta} \theta^l(x_o, \delta, \sigma_\epsilon^2) + \sigma_\epsilon^2$, the scalar σ_ϵ is the standard deviation of the measurement noise, and the expectation is with respect to $\epsilon \sim N(0, I)$. Note that the notation $\theta^{l+1}(x_o, \delta, \sigma_\epsilon^2)$ is used to emphasize that θ^l may depend on the signal x_o , the under-determinacy δ , and the measurement noise.

Let x^l denote the estimate at layer l of LDAMP/DVAMP. Our empirical findings show that the MSE of LDAMP and LDVAMP is predicted accurately by the state evolution. We formally state our finding.

Finding 1. *If the LDAMP or LDVAMP networks start from $x^0 = 0$, then for large values of m and n , state evolution predicts the mean square error of LDAMP and LDVAMP at each layer, i.e.,*

$$\theta^l(x_o, \delta, \sigma_\epsilon^2) \approx \frac{1}{n} \|x^l - x_o\|_2^2,$$

if the following conditions hold.

1. *The elements of the matrix \mathbf{A} are i.i.d. Gaussian (or subgaussian) with mean zero and standard deviation $1/m$.⁵*
2. *The noise w is also i.i.d. Gaussian.*
3. *The denoisers D^l at each layer are Lipschitz continuous.⁶*

Figure 5 demonstrates the accuracy of the state-evolution predictions under the proposed conditions.

The state evolution is a flexible tool to prove properties about D-AMP. For instance, it has been used to determine under what conditions D-AMP will recover a signal, how accurately D-AMP will recover a signal in the presence of noise, and how one should tune D-AMP [3]. In this work we use the state evolution to prove that layer-by-layer training of LDAMP/LDVAMP is MMSE optimal.

⁵The LDVAMP state evolution likely holds over a broader class of matrices, however this has not been confirmed.

⁶A denoiser is said to be L -Lipschitz continuous if for every $x_1, x_2 \in C$ we have $\|D(x_1) - D(x_2)\|_2^2 \leq L \|x_1 - x_2\|_2^2$. Convolutional denoisers are clearly Lipschitz: otherwise their gradients would explode during training.

4.2 Layer-by-layer Training is Optimal

The central challenge to using LDAMP/LDVAMP in practice is training; that is learning the network’s many free parameters. An L layer LDAMP/LDVAMP network consists of L denoisers D^1, D^2, \dots, D^L , each with their own sets of weights/parameters w^1, w^2, \dots, w^L . Together they parametrize the LDAMP/LDVAMP network with $w = [w^1, w^2, \dots, w^L]$.

In this work we test a ten layer network that uses the DnCNN denoiser at each layer. Each DnCNN denoiser is parametrized by roughly 600000 parameters. As a result, the 10 layer DnCNN-based network has over 6 million parameters to train; $w \in \mathbb{R}^{6000000}$.

Naively training such a large network is a computationally brutal task. Fortunately, the state-evolution framework allows us to prove the following powerful result: Layer-by-layer training of is MMSE optimal. We state the result formally.

Lemma 1. *Suppose that D^1, D^2, \dots, D^L are monotone denoisers in the sense that for $l = 1, 2, \dots, L$ $\inf_{w^l} \mathbb{E} \|D_{w^l(\sigma)}^l(x_o + \sigma\epsilon) - x_o\|_2^2$ is a non-decreasing function of σ . If D^1, D^2, \dots, D^L are trained to minimize $\theta^1, \theta^2, \dots, \theta^L$, respectively, then together they also minimize θ^L .*

This result follows immediately from Lemma 3 of [3].

4.3 Computational Complexity

In this section we demonstrate that in the high dimensional setting LDAMP with the DnCNN denoiser is computationally efficient.

Lemma 2. *Given a dense $m \times n$ measurement matrix \mathbf{A} with i.i.d. Gaussian distributed elements, in the high dimensional setting LDAMP with L layers and the DnCNN denoiser is no more than $2L + 1$ times slower than any other recovery algorithm that performs a matrix multiply with \mathbf{A} .*

Proof. The computational complexity of the DnCNN version of LDAMP is dominated by $2L$ matrix multiplies and $2L$ denoiser operations. Each DnCNN denoiser convolves $\sqrt{n} \times \sqrt{n} \times 64$ feature maps with $3 \times 3 \times 64$ filters, which has a computational complexity $O(n \log n)$. Each matrix multiply has a computational complexity of $O(mn)$. Thus the computational complexity of the DnCNN version of LDAMP is $O(2Lmn + Ln \log n)$. With $m > \log n$, for large m and n the computational complexity of the DnCNN version of LDAMP is less than $O((2L + 1)mn)$. \square

5 Experiments

In this section we describe how we implemented, trained, and tested LDAMP, LDVAMP, and LDIT.

5.1 Implementation

We implemented LDAMP, LDVAMP, and LDIT, using the DnCNN denoiser [32], with both TensorFlow and MatConvnet [42], which is a toolbox for Matlab. With the measurement matrices used in this section, LDVAMP had performance nearly identical to that of LDAMP, and so for brevity we do not present results for LDVAMP.⁷ The MatConvnet implementation of DnCNN was provided by the its authors here <https://github.com/csxn/DnCNN>. The results reported in this section are for the MatConvnet version of the network.

5.1.1 Datasets

Training images were pulled from Berkeley’s BSD-500 dataset [43], available at <https://www2.eecs.berkeley.edu/Research/Projects/CS/vision/grouping/resources.html>. The dataset was broken into 400 training images, 50 validation images, and 50 test images. The training images were cropped, rescaled, flipped, and rotated to form a set of 382,464 overlapping 50×50 patches. The validation images were cropped to form 6,528 non-overlapping 50×50 patches.

⁷For measurement matrices which are right rotationally invariant but not i.i.d. subgaussian the performance of LDVAMP should significantly exceed that of LDAMP.

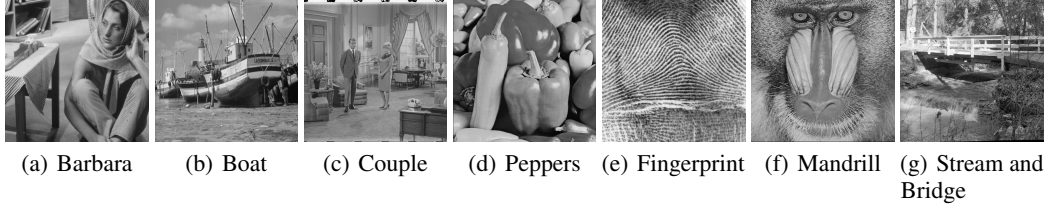


Figure 6: The seven images used for testing.

The testing results presented here are for six standard test images, illustrated in Figure 6. These images were pulled from <http://sipi.usc.edu/database/database.php?volume=misc&image=5#top> and <http://www.io.csic.es/PagsPers/JPortilla/image-processing/bls-gsm/63-test-images>. (Results for the set of 50 BSD test images are forthcoming.)

5.2 Training

We trained the LDAMP and LDIT network using the Adam optimizer [44]. We used a training rate of .001, which we dropped to .0001 and then .00001 when the validation error stopped improving. We used mini-batches of 256 patches.

We experimented with training the network in three different ways. (1) We trained the network end-to-end; we fed training data through the entire network and updated all the weights simultaneously. This training method was slow, became overfit for certain problem dimensions, and generally yielded poor performance. (2) We trained the network in a layer-by-layer fashion; we optimized the first layers weights, fixed these weights, optimized the next layer, etc. This produced good results, but the resulting network became specific to certain sampling rates and noise levels. (3) We trained ten denoisers independently; we decoupled the denoisers from the rest of the network and trained each on AWGN denoising problems at different noise levels. During inference the network used its estimate of the standard deviation of the noise to select which set of denoiser weights to use. This method produced the most flexible and highest performing network. In this section we report the results for networks trained using method (3).

The networks were trained and tested on a desktop computer with a 6 core Intel Core i7 6800k CPU and an Nvidia Pascal Titan X. Training generally took between 3 and 5 hours per denoiser network.

5.3 Testing

In this section we compare the performance of LDAMP to three state-of-the-art image recovery algorithms; TVAL3, NLR-CS, and BM3D-AMP. We also include a comparison with LDIT to demonstrate the necessity of the Onsager correction term.

5.3.1 Competing Methods

TVAL3 is an extremely fast total variation based recovery algorithm [20]. While some algorithms which use better priors are more accurate, few are faster. NLR-CS is a slow but very accurate compressive recovery algorithm [22]. With the exception of BM3D-SAPCA-AMP [3] and perhaps generative NN techniques [9], which are both impractically slow, NLR-CS is the most accurate compressive recovery algorithm. BM3D-AMP [3] (and BM3D-VAMP [11]) perform reconstructions nearly as accurately as NLR-CS and run faster than TVAL3 when dealing with Gaussian measurements.

All algorithms used their default parameters. However, NLR-CS was initialized using 8 iterations of BM3D-AMP, as described in [3]. BM3D-AMP was run for 10 iterations. LDIT and LDAMP used 10 layers. LDIT had its per iteration noise standard deviation estimate $\hat{\sigma}$ parameter set to $2\|z^t\|_2/\sqrt{m}$, as was done with BM3D-IT in [3].

Our results do not yet include comparisons with any other NN based techniques. While many NN-based methods are very specialized and only work for fixed matrices and/or block-based measurements [4–8], two recently proposed methods can be applied more generally [9; 10]. We are performing more comparisons and this manuscript will be updated with additional results.

5.3.2 Test Settings

We tested the algorithms with i.i.d. Gaussian measurements and with measurements from a randomly sampled coded diffraction pattern [45]. The coded diffraction pattern forward operator was formed as a composition of three steps; randomly change the phase, take a 2D FFT, and then randomly (uniformly) subsample.

Except for the results in Figure 7, we tested the algorithms with 128×128 images ($n = 128^2$). We report recovery accuracy in terms of PSNR.⁸ We report recovery times in seconds. All results, except for those in Figure 7, are the average taken over five distinct realizations of the measurement matrices.

5.3.3 Noise-free Recovery Results

In this section we compare all five algorithms, on all seven test images, at five different sampling rates, with both Gaussian and coded diffraction measurements.

Table 1 demonstrates that with noise-free Gaussian measurements the proposed LDAMP network produces the best reconstructions of most images at most sampling rates. The one image LDAMP consistently fails to reconstruct is Fingerprints, which looks very unlike the natural images the network was trained on.

Table 2 demonstrates that with noise-free Gaussian measurements LDIT and D-AMP produce reconstructions significantly faster than competing methods. Note that despite having to perform twice as many denoising operations, at 25% sampling the LDAMP network is only about 25% slower than LDIT. This indicates that matrix multiplies, not denoising operations, are the dominant source of computations.

Table 3 demonstrates that with coded diffraction measurements the LDAMP network again produces the best reconstructions. With these measurements as well, the network struggles to reconstruct Fingerprints.

Table 4 demonstrates that LDIT and D-AMP produce reconstructions significantly faster than competing methods. Note that because the coded diffraction measurement forward and backward operator can be applied in $O(n \log n)$ operations denoising becomes the dominant source of computations: LDAMP, which has twice as many denoising operations as LDIT, takes roughly $2\times$ longer to complete.

We end this section with a visual comparison of 512×512 reconstructions from TVAL3, BM3D-AMP, and LDAMP, presented in Figure 7. At high resolutions the LDAMP reconstructions are only incrementally better than those of BM3D-AMP, but they are computed over $60\times$ faster.

5.3.4 Noisy Recovery Results

In this section we compare TVAL3, BM3D-AMP, and LDAMP on the Boat test image at five different sampling rates, with Gaussian measurements. We chose to omit NLR-CS from these tests because [3] demonstrated that in the presence of noise BM3D-AMP significantly outperforms NLR-CS.

Table 5 demonstrates that under the aforementioned conditions LDAMP uniformly outperforms the other methods.

6 Conclusions

In this work we have developed, analyzed, and validated novel neural network architectures that mimic the behavior of the D-AMP and D-VAMP signal recovery algorithms. The LDAMP/LDVAMP networks are easy to train, can be applied to a variety of different measurement matrices, and come with a state-evolution heuristic that accurately predicts their performance. Most importantly, LDAMP outperforms the state-of-the-art BM3D-AMP and NLR-CS algorithms in terms of both accuracy and runtime.

⁸PSNR stands for peak signal-to-noise ratio and is defined as $10 \log_{10}(\frac{255^2}{\text{mean}((\hat{x}-x_o)^2)})$ when the pixel range is 0 to 255.



(a) Original Image



(b) TVAL3 (26.4 dB, 6.85 sec)



(c) BM3D-AMP (27.2 dB, 75.04 sec)



(d) LDAMP (28.1 dB, 1.22 sec)

Figure 7: Reconstructions of 5% sampled 512×512 Boat test image with coded diffraction pattern measurements and no measurement noise. LDAMP's reconstructions are noticeable better and far faster than the competing methods' reconstructions.

LDAMP/LDVAMP represent the latest example in a trend towards using training data (and lots of offline computations) to improve the performance of iterative algorithms. The key idea behind this paper is that, rather than training a fairly arbitrary “black box” to learn to recover signals, we can unroll a conventional iterative algorithm and treat the result as a NN, which produces a network with well-understood behavior, performance guarantees, and predictable shortcomings. It is our hope this paper highlights the benefits of this approach and encourages future research in this direction.

References

- [1] E. J. Candes, J. Romberg, and T. Tao, “Robust uncertainty principles: exact signal reconstruction from highly incomplete frequency information,” *IEEE Trans. Inform. Theory*, vol. 52, no. 2, pp. 489–509, Feb. 2006.
- [2] R. G. Baraniuk, “Compressive sensing [lecture notes],” *IEEE signal processing magazine*, vol. 24, no. 4, pp. 118–121, 2007.
- [3] C. A. Metzler, A. Maleki, and R. G. Baraniuk, “From denoising to compressed sensing,” *IEEE Transactions on Information Theory*, vol. 62, no. 9, pp. 5117–5144, 2016.

Table 1: PSNR of 128×128 reconstructions with i.i.d. Gaussian measurements and no measurement noise.

5% Sampling	Barbara	Boat	Fingerprint	Mandrill	Peppers	Couple	Stream & Bridge
TVAL3	19.32	21.05	16.49	21.98	19.36	21.09	19.22
BM3D-AMP	18.04	24.04	12.25	24.12	18.28	24.79	16.77
LDIT	17.20	19.37	16.94	20.43	17.49	19.51	18.08
LDAMP	21.26	22.44	17.04	22.84	21.30	22.74	20.17
NLR-CS	20.31	21.51	14.96	22.05	19.69	21.55	19.22
10% Sampling	Barbara	Boat	Fingerprint	Mandrill	Peppers	Couple	Stream & Bridge
TVAL3	21.75	22.95	16.77	23.21	21.98	23.07	20.86
BM3D-AMP	24.36	24.04	18.07	24.12	24.44	24.79	22.05
LDIT	19.39	21.49	17.23	22.17	19.13	21.24	19.82
LDAMP	25.80	24.67	17.36	24.37	26.00	25.43	22.52
NLR-CS	25.17	23.84	17.84	23.56	25.18	24.91	21.80
15% Sampling	Barbara	Boat	Fingerprint	Mandrill	Peppers	Couple	Stream & Bridge
TVAL3	23.47	24.25	16.97	24.09	24.18	24.74	22.00
BM3D-AMP	27.35	25.67	19.94	25.02	27.37	26.96	23.35
LDIT	20.53	22.54	17.29	23.17	19.74	21.89	19.50
LDAMP	28.78	26.79	17.65	25.40	29.38	27.65	23.97
NLR-CS	28.10	25.57	20.11	24.45	28.06	26.82	23.10
20% Sampling	Barbara	Boat	Fingerprint	Mandrill	Peppers	Couple	Stream & Bridge
TVAL3	25.20	25.47	17.32	24.84	25.90	26.17	23.08
BM3D-AMP	29.57	27.40	21.19	25.80	29.55	28.55	24.45
LDIT	20.42	22.50	17.34	22.66	21.45	22.29	20.95
LDAMP	31.10	28.58	18.07	26.31	31.88	29.57	25.21
NLR-CS	32.42	28.78	22.04	26.52	32.47	30.13	25.26
25% Sampling	Barbara	Boat	Fingerprint	Mandrill	Peppers	Couple	Stream & Bridge
TVAL3	26.57	26.53	17.62	25.46	27.49	27.44	23.98
BM3D-AMP	31.39	28.89	21.97	26.50	31.27	30.01	25.37
LDIT	21.59	23.02	17.57	23.61	21.65	23.22	21.04
LDAMP	32.68	30.17	18.13	27.06	33.87	31.06	26.20
NLR-CS	32.42	28.78	22.04	26.52	32.47	30.13	25.26

Table 2: Runtimes (seconds) of 128×128 reconstructions with i.i.d. Gaussian measurements and no measurement noise.

Sampling Rate	5%	10%	15%	20%	25%
TVAL3	1.36	2.24	2.87	3.58	4.33
BM3D-AMP	3.85	4.80	4.45	4.24	4.10
LDIT	0.21	0.28	0.36	0.42	0.48
LDAMP	0.34	0.40	0.49	0.55	0.61
NLR-CS	67.83	85.91	103.87	124.35	146.29

Table 3: PSNR of 128×128 reconstructions with coded diffraction measurements and no measurement noise.

5% Sampling	Barbara	Boat	Fingerprint	Mandrill	Peppers	Couple	Stream & Bridge
TVAL3	21.66	22.70	16.79	23.20	21.94	22.98	20.92
BM3D-AMP	18.37	24.48	13.46	24.48	17.80	25.53	20.83
LDIT	20.20	21.09	16.69	22.31	19.07	20.85	19.98
LDAMP	22.10	23.45	17.33	23.54	22.32	23.50	20.94
NLR-CS	15.14	13.44	11.73	18.43	17.23	17.70	16.04
10% Sampling	Barbara	Boat	Fingerprint	Mandrill	Peppers	Couple	Stream & Bridge
TVAL3	25.08	25.39	17.34	24.79	25.83	26.13	23.13
BM3D-AMP	25.40	24.48	18.68	24.48	25.52	25.53	22.56
LDIT	24.02	24.77	17.31	24.74	24.36	25.24	20.21
LDAMP	27.90	26.50	17.56	25.57	28.18	27.24	23.87
NLR-CS	24.12	21.56	17.11	21.15	24.05	22.27	21.04
15% Sampling	Barbara	Boat	Fingerprint	Mandrill	Peppers	Couple	Stream & Bridge
TVAL3	27.78	27.71	17.96	26.05	28.90	28.54	24.90
BM3D-AMP	28.96	25.98	20.39	25.12	28.67	27.11	23.63
LDIT	28.44	26.59	17.31	25.73	30.21	26.92	24.28
LDAMP	30.85	28.79	17.86	26.68	32.07	29.54	25.69
NLR-CS	27.35	24.16	18.99	23.28	21.24	24.23	20.58
20% Sampling	Barbara	Boat	Fingerprint	Mandrill	Peppers	Couple	Stream & Bridge
TVAL3	30.05	29.93	18.73	27.32	31.62	30.77	26.55
BM3D-AMP	32.08	28.07	21.41	25.89	31.47	28.99	24.57
LDIT	31.60	28.61	17.30	26.06	32.15	30.49	25.57
LDAMP	33.10	30.20	17.94	27.59	34.06	32.17	27.24
NLR-CS	31.74	28.16	20.64	25.79	28.60	28.89	21.04
25% Sampling	Barbara	Boat	Fingerprint	Mandrill	Peppers	Couple	Stream & Bridge
TVAL3	32.37	32.13	19.63	28.63	34.20	33.05	28.12
BM3D-AMP	34.69	29.59	22.26	26.36	34.74	30.51	25.69
LDIT	34.00	30.43	17.65	26.24	35.37	31.02	27.63
LDAMP	34.58	32.62	18.60	29.01	36.07	33.86	28.60
NLR-CS	31.74	28.16	20.64	25.79	28.60	28.89	21.04

Table 4: Runtimes (seconds) of 128×128 reconstructions with coded diffraction measurements and no measurement noise.

Sampling Rate	5%	10%	15%	20%	25%
TVAL3	0.62	0.52	0.46	0.43	0.41
BM3D-AMP	3.80	4.55	4.29	3.67	3.40
LDIT	0.13	0.14	0.14	0.14	0.14
LDAMP	0.26	0.26	0.26	0.27	0.26
NLR-CS	87.26	87.82	87.43	87.18	86.87

Table 5: PSNR of reconstruction of 128×128 Boat test image with additive white Gaussian measurement noise (AWGN) with various standard deviations (s.d.).

AWGN with s.d. 10					
Sampling rate (%)	10	20	30	40	50
TVAL3	21.08	22.84	24.06	24.97	25.75
BM3D-AMP	16.99	23.98	25.40	26.79	27.64
LDAMP	22.41	24.56	26.36	27.62	28.56
AWGN with s.d. 20					
Sampling Rate (%)	10	20	30	40	50
TVAL3	21.00	22.60	23.50	23.94	24.16
BM3D-AMP	21.03	23.67	24.63	25.45	26.03
LDAMP	22.33	24.24	25.35	26.33	26.75
AWGN with s.d. 30					
Sampling Rate (%)	10	20	30	40	50
TVAL3	20.90	22.23	22.74	22.74	22.57
BM3D-AMP	18.43	23.34	24.09	24.46	24.80
LDAMP	22.11	23.80	24.55	25.10	25.34
AWGN with s.d. 40					
Sampling Rate (%)	10	20	30	40	50
TVAL3	20.77	21.80	21.93	21.60	21.12
BM3D-AMP	19.24	23.02	23.55	23.77	23.94
LDAMP	21.85	23.41	23.90	24.33	24.50
AWGN with s.d. 50					
Sampling Rate (%)	10	20	30	40	50
TVAL3	20.58	21.33	21.17	20.53	19.84
BM3D-AMP	19.45	22.69	23.13	23.28	23.38
LDAMP	21.58	22.96	23.44	23.65	23.76

- [4] A. Mousavi, A. B. Patel, and R. G. Baraniuk, "A deep learning approach to structured signal recovery," in *Communication, Control, and Computing (Allerton), 2015 53rd Annual Allerton Conference on*. IEEE, 2015, pp. 1336–1343.
- [5] K. Kulkarni, S. Lohit, P. Turaga, R. Kerviche, and A. Ashok, "Reconnet: Non-iterative reconstruction of images from compressively sensed random measurements," *arXiv preprint arXiv:1601.06892*, 2016.
- [6] A. Mousavi and R. G. Baraniuk, "Learning to invert: Signal recovery via deep convolutional networks," *arXiv preprint arXiv:1701.03891*, 2017.
- [7] H. Yao, F. Dai, D. Zhang, Y. Ma, S. Zhang, and Y. Zhang, "DR²-net: Deep residual reconstruction network for image compressive sensing," *arXiv preprint arXiv:1702.05743*, 2017.
- [8] Y. Yang, J. Sun, H. Li, and Z. Xu, "Deep admm-net for compressive sensing mri," *Advances in Neural Information Processing Systems*, vol. 29, pp. 10–18, 2016.
- [9] A. Dave, A. K. Vadathya, and K. Mitra, "Compressive image recovery using recurrent generative model," *arXiv preprint arXiv:1612.04229*, 2016.
- [10] J. Chang, C.-L. Li, B. Póczos, B. Kumar, and A. C. Sankaranarayanan, "One network to solve them all—solving linear inverse problems using deep projection models," *arXiv preprint arXiv:1703.09912*, 2017.
- [11] P. Schniter, S. Rangan, and A. Fletcher, "Denoising based vector approximate message passing," *arXiv preprint arXiv:1611.01376*, 2016.
- [12] K. Gregor and Y. LeCun, "Learning fast approximations of sparse coding," in *Proceedings of the 27th International Conference on Machine Learning (ICML-10)*, 2010, pp. 399–406.

- [13] U. S. Kamilov and H. Mansour, "Learning optimal nonlinearities for iterative thresholding algorithms," *IEEE Signal Process. Lett.*, vol. 23, no. 5, pp. 747–751, 2016.
- [14] M. Borgerding and P. Schniter, "Onsager-corrected deep networks for sparse linear inverse problems," *arXiv preprint arXiv:1612.01183*, 2016.
- [15] I. Daubechies, M. Defrise, and C. D. Mol, "An iterative thresholding algorithm for linear inverse problems with a sparsity constraint," *Comm. on Pure and Applied Math.*, vol. 75, pp. 1412–1457, 2004.
- [16] D. L. Donoho, A. Maleki, and A. Montanari, "Message passing algorithms for compressed sensing," *Proc. Natl. Acad. Sci.*, vol. 106, no. 45, pp. 18 914–18 919, 2009.
- [17] S. Rangan, P. Schniter, and A. Fletcher, "Vector approximate message passing," *arXiv preprint arXiv:1610.03082*, 2016.
- [18] E. J. Candes and T. Tao, "Decoding by linear programming," *IEEE Trans. Inform. Theory*, vol. 51, no. 12, pp. 4203 – 4215, Dec. 2005.
- [19] D. Needell and J. A. Tropp, "Cosamp: Iterative signal recovery from incomplete and inaccurate samples," *Appl. Comput. Harmon. Anal.*, vol. 26, no. 3, pp. 301–321, 2009.
- [20] C. Li, W. Yin, and Y. Zhang, "User's guide for tval3: Tv minimization by augmented lagrangian and alternating direction algorithms," *CAAM report*, vol. 20, pp. 46–47, 2009.
- [21] R. G. Baraniuk, V. Cevher, M. F. Duarte, and C. Hegde, "Model-based compressive sensing," *IEEE Trans. Inform. Theory*, vol. 56, no. 4, pp. 1982 –2001, Apr. 2010.
- [22] W. Dong, G. Shi, X. Li, Y. Ma, and F. Huang, "Compressive sensing via nonlocal low-rank regularization," *to appear in IEEE Trans. Image Processing*, 2014.
- [23] S. Beygi, S. Jalali, A. Maleki, and U. Mitra, "An efficient algorithm for compression-based compressed sensing," *arXiv preprint arXiv:1704.01992*, 2017.
- [24] E. W. Tramel, A. Drémeau, and F. Krzakala, "Approximate message passing with restricted boltzmann machine priors," *Journal of Statistical Mechanics: Theory and Experiment*, vol. 2016, no. 7, p. 073401, 2016.
- [25] E. W. Tramel, A. Manoel, F. Caltagirone, M. Gabrié, and F. Krzakala, "Inferring sparsity: Compressed sensing using generalized restricted boltzmann machines," in *Information Theory Workshop (ITW), 2016 IEEE*. IEEE, 2016, pp. 265–269.
- [26] E. W. Tramel, M. Gabrié, A. Manoel, F. Caltagirone, and F. Krzakala, "A deterministic and generalized framework for unsupervised learning with restricted boltzmann machines," *arXiv preprint arXiv:1702.03260*, 2017.
- [27] L. Theis and M. Bethge, "Generative image modeling using spatial lstms," in *Advances in Neural Information Processing Systems*, 2015, pp. 1927–1935.
- [28] S. Boyd, N. Parikh, E. Chu, B. Peleato, and J. Eckstein, "Distributed optimization and statistical learning via the alternating direction method of multipliers," *Foundations and Trends® in Machine Learning*, vol. 3, no. 1, pp. 1–122, 2011.
- [29] S. V. Venkatakrisnan, C. A. Bouman, and B. Wohlberg, "Plug-and-play priors for model based reconstruction," in *Global Conference on Signal and Information Processing (GlobalSIP), 2013 IEEE*. IEEE, 2013, pp. 945–948.
- [30] J. R. Hershey, J. L. Roux, and F. Weninger, "Deep unfolding: Model-based inspiration of novel deep architectures," *arXiv preprint arXiv:1409.2574*, 2014.
- [31] T. B. Yakar, P. Sprechmann, R. Litman, A. M. Bronstein, and G. Sapiro, "Bilevel sparse models for polyphonic music transcription," in *ISMIR*, 2013, pp. 65–70.
- [32] K. Zhang, W. Zuo, Y. Chen, D. Meng, and L. Zhang, "Beyond a gaussian denoiser: Residual learning of deep cnn for image denoising," *IEEE Transactions on Image Processing*, 2017.
- [33] K. Dabov, A. Foi, V. Katkovnik, and K. Egiazarian, "Image denoising by sparse 3-d transform-domain collaborative filtering," *IEEE Trans. Image Processing*, vol. 16, no. 8, pp. 2080–2095, Aug. 2007. [Online]. Available: <http://dx.doi.org/10.1109/TIP.2007.901238>

- [34] M. Figueiredo, R. Nowak, and S. Wright, “Gradient projection for sparse reconstruction: Application to compressed sensing and other inverse problems,” *IEEE J. Select. Top. Signal Processing*, vol. 1, no. 4, pp. 586–598, 2007.
- [35] A. Maleki, “Approximate message passing algorithm for compressed sensing,” *Stanford University PhD Thesis*, Nov. 2010.
- [36] S. Ramani, T. Blu, and M. Unser, “Monte-carlo sure: A black-box optimization of regularization parameters for general denoising algorithms,” *IEEE Trans. Image Processing*, pp. 1540–1554, 2008.
- [37] H. C. Burger, C. J. Schuler, and S. Harmeling, “Image denoising: Can plain neural networks compete with bm3d?” in *Computer Vision and Pattern Recognition (CVPR), 2012 IEEE Conference on*. IEEE, 2012, pp. 2392–2399.
- [38] A. Krizhevsky, I. Sutskever, and G. E. Hinton, “Imagenet classification with deep convolutional neural networks,” in *Advances in neural information processing systems*, 2012, pp. 1097–1105.
- [39] S. Ioffe and C. Szegedy, “Batch normalization: Accelerating deep network training by reducing internal covariate shift,” *arXiv preprint arXiv:1502.03167*, 2015.
- [40] K. He, X. Zhang, S. Ren, and J. Sun, “Deep residual learning for image recognition,” in *Proceedings of the IEEE Conference on Computer Vision and Pattern Recognition*, 2016, pp. 770–778.
- [41] M. Bayati and A. Montanari, “The dynamics of message passing on dense graphs, with applications to compressed sensing,” *IEEE Trans. Inform. Theory*, vol. 57, no. 2, pp. 764–785, 2011.
- [42] A. Vedaldi and K. Lenc, “Matconvnet – convolutional neural networks for matlab,” in *Proceeding of the ACM Int. Conf. on Multimedia*, 2015.
- [43] D. Martin, C. Fowlkes, D. Tal, and J. Malik, “A database of human segmented natural images and its application to evaluating segmentation algorithms and measuring ecological statistics,” in *Proc. 8th Int’l Conf. Computer Vision*, vol. 2, July 2001, pp. 416–423.
- [44] D. Kingma and J. Ba, “Adam: A method for stochastic optimization,” *arXiv preprint arXiv:1412.6980*, 2014.
- [45] E. J. Candes, X. Li, and M. Soltanolkotabi, “Phase retrieval from coded diffraction patterns,” *Applied and Computational Harmonic Analysis*, vol. 39, no. 2, pp. 277–299, 2015.